Optics Letters

Rotational echo spectroscopy for accurate measurement of molecular alignment

Pu Wang,[1,2] Lixin He,[1,2,3] Yanqing He,[1,2] Jianchang Hu,[1,2] Siqi Sun,[1,2] Pengfei Lan,[1,2,4] and Peixiang Lu[1,2]

[1]Wuhan National Laboratory for Optoelectronics and School of Physics, Huazhong University of Science and Technology, Wuhan 430074, China
[2]Optical Valley Laboratory, Hubei 430074, China
[3]e-mail:helx_hust@mail.hust.edu.cn
[4]e-mail: pengfeilan@mail.hust.edu.cn

Received 13 December 2021; revised 17 January 2022; accepted 20 January 2022; posted 20 January 2022; published 16 February 2022

We measure the molecular alignment induced in gas using molecular rotational echo spectroscopy. Our results show that the echo intensity and the time interval between the local extremas of the echo responses depend sensitively on the pump intensities and the initial molecular rotational temperature, respectively. This allows us to accurately extract these experimental parameters from the echo signals and then further determine the molecular alignment in experiments. The accuracy of our method has been verified by comparing the simulation with the extracted parameters from the molecular alignment experiment performed with a femtosecond pump pulse.

https://doi.org/10.1364/OL.451011

Molecular alignment plays an important role in probing the molecular reaction and collision dynamics. Over the past decades, molecular alignment in various molecules has been successfully achieved via the interaction with a femtosecond laser pulse [1–6]. Recently, widespread applications of molecular alignment have been implemented in many areas, varying from multiphoton ionization [7,8], ultrashort pulse compression [9,10], molecular orbital reconstruction [11–13], control and imaging of chemical reactions [14–16], and high harmonic generation (HHG) [17–24]. To date, it is still a challenge to achieve perfect molecular alignment in experiments. For the partial molecular alignment, the measured results are averaged over the molecular alignment distribution. Hence, an accurate measurement of the molecular alignment in the experiment is essential for probing the molecular dynamics and structure in the molecular frame. In the molecular alignment experiment, the induced rotational dynamics is determined by the initial molecular rotational temperature and the laser parameters (e.g., pulse duration, laser frequency, pump intensity) at the interaction region. The initial molecular rotational temperature determines the initial thermal distribution of the molecular rotational states and the pump pulse determines the redistribution of the rotational states after the laser–molecule interaction. For the comprehensive description of the molecular alignment, it is necessary to accurately measure these parameters in the experiment. Previously, it was reported that the molecular rotational temperature can be measured by coherent anti-Stokes Raman scattering (CARS) [25–27] and degenerate four-wave mixing (DFWM) [28]. However, these methods are limited by the frequency of the signal. As an alternative, Yoshii *et al.* demonstrated that the initial molecular rotational temperature can be determined by comparing the Fourier spectrum of the time-dependent HHG signals with the theory [29]. However, their method assumes that the laser parameters in experiments are known. Although the pulse duration and the laser frequency can be easily measured by an optical autocorrelator and spectrometer, respectively, the laser intensity at the interaction region is difficult to accurately estimated in the experiment. Very recently, He *et al.* reported that the initial molecular rotational temperature and the pump laser intensity can be simultaneously extracted from the arising time of the extremas of the time-dependent HHG signals of aligned molecules [30]. However, the molecular HHG experiment requires complex experimental setups, and limits the molecular gas density and rotational temperature to a lower level. Moreover, the HHG spectrum encodes the information of the molecular structures [11–13]. For the molecules with complex structures, the arising time of the extremas of the time-dependent HHG signals will be obstructed. Therefore, an accurate and widely applicable method to measure the molecular alignment is still desired.

Recently, a new type of molecular alignment response known as "molecular alignment echo" was reported [31–41]. Excited by two laser pulses delayed by $\Delta\tau$, an alignment response will appear at the time delay of $\Delta t = 2\Delta\tau$ after the first excitation pulse. This phenomenon is called "molecular alignment echo." A typical echo response can be seen in the time-dependent curve of alignment factor $\langle\cos^2\theta\rangle(t)$, as shown in Fig. 1(a). Since the first discovery of the molecular alignment echo in CO_2 molecules, many studies have been reported to explain the formation mechanism of the alignment echo [31–38]. Recently, high-order fractional alignment echo [33–36], imaginary echo [34,35], and rotational echo [34,35] have also been observed, and the application of the alignment echo to probe the molecular collision dynamics has also been demonstrated [32,41].

In this work, we demonstrate that the laser-induced molecular alignment in gas can be accurately measured by molecular

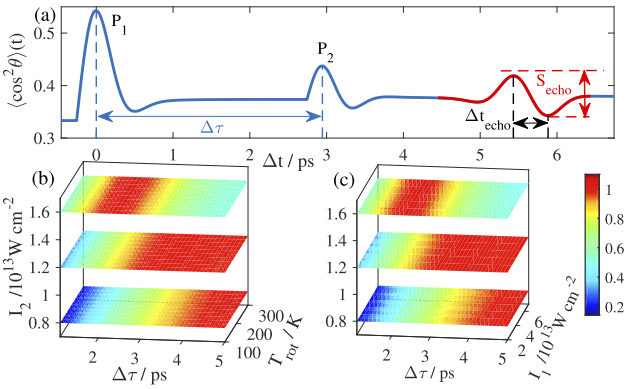

Fig. 1. (a) Time-dependent mean value of $\langle\cos^2\theta\rangle$ calculated with the N_2O molecule excited by two pump pulses. Here, the initial molecular rotational temperature is 100 K, the intensities of P_1 and P_2 are 5×10^{13} W/cm^2 and 2×10^{13} W/cm^2, respectively. (b) TDSE simulations of $\Delta\tau$-dependent alignment echo intensity as a function of T_{rot} for different I_2. Here, $I_1 = 2\times10^{13}$ W/cm^2 and the $\Delta\tau$-dependent echo intensity for the same T_{rot} is normalized by its maximum. (c) Normalized $\Delta\tau$-dependent echo intensity as a function of I_1 for different I_2. Here, the initial molecular rotational temperature is 100 K.

alignment echo spectroscopy. Our simulations reveal the unique dependence of the echo intensity and the time interval between the local extremas of the echo response on the pump intensities and the initial molecular rotational temperature, respectively. With this unique feature, we have successfully measured the pump intensities and the initial molecular rotational temperature in the experiment. The accuracy of the proposed method was verified by comparing the simulations with the extracted parameters to the molecular alignment experiment performed with a single pump pulse. Our simulations and experimental results are in good agreement. This method is decoupled from the other experimental parameters such as the gas density and the interaction length between the pump pulse and the probe pulse, which makes it a flexible method for many molecular alignment experimental setups.

We first measure the pump intensity with the molecular alignment echo. In Figs. 1(b) and 1(c), we calculate the $\Delta\tau$-dependent echo intensity as a function of the intensity of the first pump pulses (I_1) and the initial molecular rotational temperature (T_{rot}) for different second pump intensity (I_2). Here, the $\Delta\tau$-dependent echo intensity for the same T_{rot} and I_1 has been normalized by its maximum. Our simulations are performed by solving the time-dependent Schrödinger equation (TDSE) of the molecular rotational wave packet [42]. In our calculations, we choose N_2O as the target molecule, which has a long revival period (T_{rev} ~ 39.78 ps) without quarter revivals, and can provide a broad time window for studying the echo phenomena. In our simulation, we characterize the peak-to-peak difference of the echo response [see Fig. 1(a)] in the $\langle\cos^2\theta\rangle(t)$ as the intensity of the echo signal. From Figs. 1(b) and 1(c), one can see that the normalized $\Delta\tau$-dependence of the echo intensity is only determined by I_2 and is independent of I_1 and T_{rot}. The intricate dependence of the echo intensity on the pump intensities and $\Delta\tau$ can be attributed to the interference of multiple quantum pathways in the multilevel rotational system [37–40], which is decoupled from the laboratorial parameters such as the gas density and the interaction length between the pump pulse and the probe pulse. This unique feature can be used to extract the two pump intensities from the measurements.

With the above idea, we have performed an experiment to measure the molecular alignment echo signals. This experiment is implemented with the schematic depicted in Fig. 2(a). The laser source is a commercial Ti:sapphire laser system (Astrella-USP-1K, Coherent, Inc.). It delivers Gaussian laser pulses at a repetition rate of 1 kHz. The pulse duration and the central wavelength are 35 fs and 800 nm, respectively. The output laser pulse is divided into three optical paths by two beam splitters. The two pump pulses (P_1 and P_2) are linearly polarized in the same direction and the time delay $\Delta\tau$ between them is adjusted by a computer controlled translation stage. The probe pulse is frequency doubled via a BBO crystal and the remaining output from the 800-nm laser is filtered by a bandpass filter centered at 400 nm. The time delay Δt between the probe pump and P_2 is controlled by the second motorized translation stage. The probe pulse is polarized by a polarizer and set to $-\pi/4$ [see Fig. 2(a)] with respect to the pump pulses. These three pulses are focused into a gas cell by a concave mirror (f=400 mm) in the collinear geometry. The diameter of the focal spot of the pump pulse is approximately 160 μm. N_2O is injected into the gas cell through a nozzle with a diameter of 500 μm. The gas pressures within the nozzle and the gas cell are 2.5×10^5 Pa and 9.83×10^4 Pa, respectively. The distance between the gas exit and the optical axis is 1 mm. The alignment echoes are measured by the time-resolved birefringence signal as in [31,43]. The birefringence signal measured on the detector can be written as

$$I_{signal}(t) \propto \left[\langle\cos^2\theta\rangle(t) - 1/3\right]^2. \quad \textbf{(1)}$$

In our experiment, we record the time-dependent birefringence signals for different $\Delta\tau$. The powers of P_1 and P_2 are measured to be 145 mW and 70 mW (estimated intensities are 2.16×10^{13} W/cm^2 and 1.04×10^{13} W/cm^2), respectively. Figure 2(b) depicts the echo signals measured at different $\Delta\tau$. Figure 2(c) plots the corresponding echo intensities (red circles) as a function of $\Delta\tau$. In Fig. 1, we have proved that the normalized $\Delta\tau$-dependence of the echo intensity is only determined by I_2. We have calculated the $\Delta\tau$-dependent echo intensities for different I_2. By minimizing the root-mean-square error (RMSE) between the measurements and the simulations, the intensity of P_2 is extracted as $I_2 = 1.3\pm0.05\times10^{13}$ W/cm^2. Here the uncertainty is estimated so that the R^2 factor of the fit is larger than 0.9. This method can also be used to determine the intensity of P_1 if we exchange the sequence of P_1 and P_2. Figures 2(d) and 2(e) depict the measured time-dependent signals and the corresponding normalized $\Delta\tau$-dependent echo intensities with P_1 after P_2. In this case, the extracted intensity of P_1 is $1.95\pm0.05\times10^{13}$ W/cm^2. Note that in our experiment, the probe pulse is focused with a smaller spot size than the pump pulses. Thus, only the central region of the pump beam is responsible for the birefringence measurement. The extracted laser intensities should be the same as that at the central region of the focal spot of the pump lasers. In addition, we have also performed the simulations with the pump intensity varying by $\pm0.1\times10^{13}$ W/cm^2 as shown in Figs. 2(c) and 2(e). One can see that these results deviate obviously from the measurements, indicating a high sensitivity of our method to the pump intensity.

With I_1 and I_2 determined, we next extract the initial molecular rotational temperature T_{rot} from the echo signals. Our simulations indicate that the time interval Δt_{echo} between the local extremas of the echo signals depends sensitively on T_{rot}.

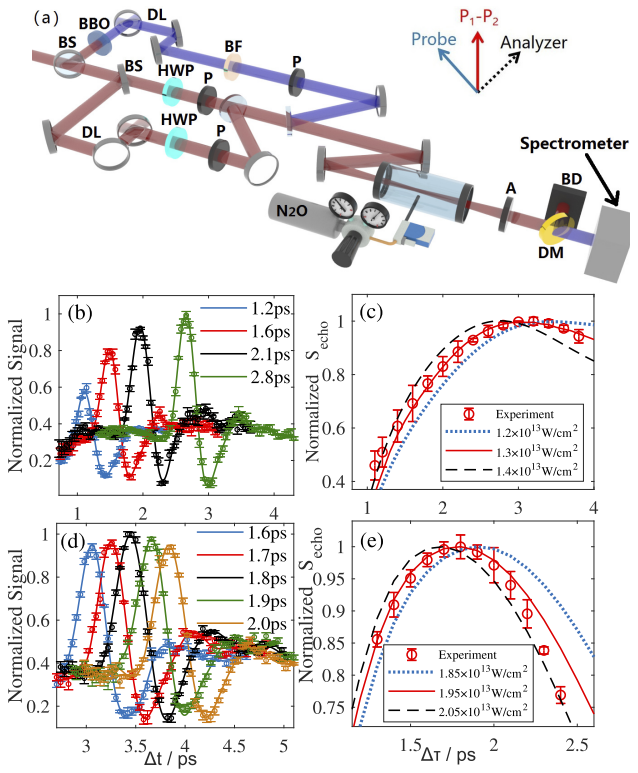

Fig. 2. (a) Schematic diagram of the experimental setup. A, Analyzer; BBO, BaB_2O_4; BD, beam dump; BF, 400-nm bandpass filter; BS, beamsplitter; DL: delay line; DM, dichroic mirror; HWP, half-wave plate; P, polarizer. The relative polarizations of the different pulses together with the orientation of the analyzer are shown in the insets. (b) Measured time-dependent echo signals for different $\Delta\tau$ with P_1 before P_2. The curves correspond to the measurements from left to right. (c) Comparison between the measured (circles) and the calculated (lines) $\Delta\tau$-dependent echo intensity. The curves correspond to the measurements from left to right. (d)–(e) Same as panels (b)–(c) but for P_1 after P_2.

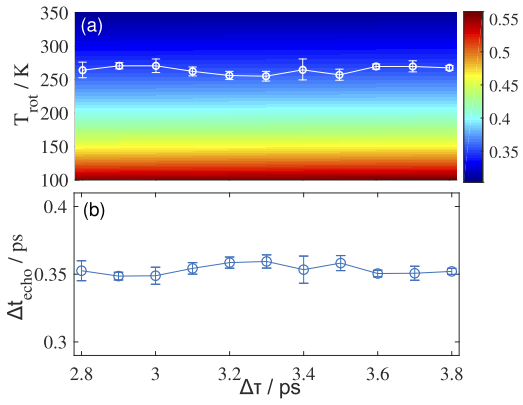

Fig. 3. (a) Simulated time interval between the local extremas of the molecular alignment echo signals as a function of T_{rot} for different $\Delta\tau$. The white curve is the initial molecular rotational temperature extracted from the experimental results. (b) Measured Δt_{echo} as a function of $\Delta\tau$ in the experiment.

Figure 3(a) depicts the calculated Δt_{echo} as a function of T_{rot} for different $\Delta\tau$. Here, the simulation is performed with the pump intensities extracted above. One can see that Δt_{echo} decreases as T_{rot} increases. Moreover, Δt_{echo} is almost independent of $\Delta\tau$. This is because the value of Δt_{echo} is determined by the barycenter of the molecular rotational state distribution [44]. As we mentioned above, the initial molecular rotational temperature determines the initial thermal distribution of the molecular rotational states and the pump pulse determines the redistribution of the rotational states after the laser–molecule interaction. The pump intensities in our experiment have been extracted from the above measurements. The initial molecular rotational temperature is the only parameter that affects Δt_{echo}. Figure 3(b) depicts the measured Δt_{echo} as a function of $\Delta\tau$. One can see that Δt_{echo} (0.35 ps) is almost the same for different $\Delta\tau$. By comparison with the simulations, the initial molecular rotational temperature can be extracted, as shown as the white curve in Fig. 3(a), which is approximately 264±6 K. In view of the experimental errors of the extracted pump intensities, we have extracted T_{rot} with the two pump intensities varying by $\pm 0.1 \times 10^{13}$ W/cm^2. Our results indicate that the variation of the extracted T_{rot} is less than 3 K within our experimental error, which indicates a weak influence of the errors of the extracted pump intensities on the extraction of T_{rot}.

We have also cross verified the extracted T_{rot} with other methods. In principle, we can compare our result to the CARS measurement. However, due to the limited spectral bandwidth of the 800-nm femtosecond laser in our experiment, which will limit the frequency range of the CARS spectrum, we did not perform the CARS experiment. As an alternative, we used a method similar to that in [29] by analyzing the Fourier spectrum of the time-dependent birefringence signal excited by P_2 alone. The extracted initial molecular rotational temperature is approximately 250 K, which is close to our result. Moreover, we have also calculated the temperature distribution in the interaction region with the FLUENT software [45]. The calculated result is 256 K. This result is also close to ours.

Finally, to verify the accuracy of our method, we performed the molecular alignment experiment with P_2 alone. The time-dependent alignment signals recorded around the 1/2 revival of N_2O are shown as the circles in Fig. 4. For comparison, the simulations with the previously extracted intensity of P_2 (1.3×10^{13} W/cm^2) and the initial molecular rotational temperature (264 K) is also presented as the solid curve in Fig. 4. One can see that the simulations are in good agreement with the experimental results, indicating the high accuracy of our method.

In conclusion, we have demonstrated a simple and accurate method to measure the molecular alignment induced in gas using

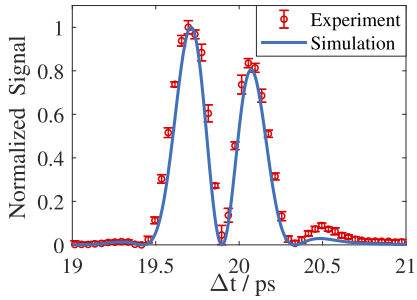

Fig. 4. Normalized molecular alignment signals (circles) measured with P_2 alone. For comparison, the result calculated with the extracted pump intensity (1.3×10^{13} W/cm^2) and the initial molecular rotational temperature (264 K) is also presented (solid curve).

molecular alignment echo spectroscopy. From the simulations, we find that the normalized $\Delta\tau$-dependence of the echo intensity is only determined by the intensity of the second pump pulse. This feature enables us to accurately measure the intensities of the pump pulses in the molecular alignment experiment. Moreover, our results reveal that the time interval between the local extremas of the echo signals depends sensitively on the initial molecular rotational temperature, which enables an accurate measurement of the initial molecular rotational temperature. We have demonstrated the accuracy of our method by comparing the simulations with the extracted parameters to the molecular alignment experiment performed with a single pump pulse. Unlike the methods in [25–29], the proposed method can simultaneously measure the pump intensities and the initial molecular rotational temperature, which allows a full characterization of the molecular alignment. Compared with the HHG method in [30] which also claims the simultaneous measurement of the pump intensity and the initial molecular rotational temperature, the proposed method does not require complex experimental setups and is not limited by the gas density. Moreover, molecular alignment echo spectroscopy can be applied not only to linear molecules, but also to asymmetric-top molecules [46], and, potentially, to liquids [32].

Funding. National Key Research and Development Program of China (2019YFA0308300); National Natural Science Foundation of China (91950202, 12074136, 11774109, 12021004); Fundamental Research Funds for the Central Universities (2017KFXKJC002); Natural Science Foundation of Hubei Province (2021CFB330); the Program for HUST Academic Frontier Youth Team.

Disclosures. The authors declare no conflicts of interest.

Data availability. Data underlying the results presented in this paper are not publicly available at this time but may be obtained from the authors upon reasonable request.

REFERENCES

1. L. Cai, J. Marango, and B. Friedrich, Phys. Rev. Lett. **86**, 775 (2001).
2. H. Stapelfeldt and T. Seideman, Rev. Mod. Phys. **75**, 543 (2003).
3. O. Ghafur, A. Rouzée, A. Gijsbertsen, W. K. Siu, S. Stolte, and M. J. J. Vrakking, Nat. Phys. **5**, 289 (2009).
4. Y. Ohshima and H. Hasegawa, Int. Rev. Phys. Chem. **29**, 619 (2010).
5. K. Lin, I. Tutunnikov, J. Qiang, J. Ma, Q. Song, Q. Ji, W. Zhang, H. Li, F. Sun, X. Gong, H. Li, P. Lu, H. Zeng, Y. Prior, I. S. Averbukh, and J. Wu, Nat. Commun. **9**, 5134 (2018).
6. E. T. Karamatskos, S. Raabe, T. Mullins, A. Trabattoni, P. Stammer, G. Goldsztejn, R. R. Johansen, K. Dlugolecki, H. Stapelfeldt, M. J. J. Vrakking, S. Trippel, A. Rouzée, and J. Küpper, Nat. Commun. **10**, 3364 (2019).
7. I. V. Litvinyuk, K. F. Lee, P. W. Dooley, D. M. Rayner, D. M. Villeneuve, and P. B. Corkum, Phys. Rev. Lett. **90**, 233003 (2003).
8. T. K. Kjeldsen, C. Z. Bisgaard, L. B. Madsen, and H. Stapelfeldt, Phys. Rev. A **68**, 063407 (2003).
9. J. Wu, H. Cai, H. Zeng, and A. Couairon, Opt. Lett. **33**, 2593 (2008).
10. R. A. Bartels, T. C. Weinacht, N. Wagner, M. Baertschy, C. H. Greene, M. M. Murnane, and H. C. Kapteyn, Phys. Rev. Lett. **88**, 013903 (2001).
11. J. Itatani, J. Levesque, D. Zeidler, H. Niikura, H. Pépin, J. C. Kieffer, P. B. Corkum, and D. M. Villeneuve, Nature **432**, 867 (2004).
12. C. Vozzi, M. Negro, F. Calegari, G. Sansone, M. Nisoli, S. De Silvestri, and S. Stagira, Nat. Phys. **7**, 822 (2011).
13. C. Zhai, X. Zhang, X. Zhu, L. He, Y. Zhang, B. Wang, Q. Zhang, P. Lan, and P. Lu, Opt. Express **26**, 2775 (2018).
14. J. J. Larsen, I. Wendt-Larsen, and H. Stapelfeldt, Phys. Rev. Lett. **83**, 1123 (1999).
15. C. Z. Bisgaard, O. J. Clarkin, G. Wu, A. M. D. Lee, O. Gessner, C. C. Hayden, and A. Stolow, Science **323**, 1464 (2009).
16. C. B. Madsen, L. B. Madsen, S. S. Viftrup, M. P. Johansson, T. B. Poulsen, L. Holmegaard, V. Kumarappan, K. A. Jørgensen, and H. Stapelfeldt, Phys. Rev. Lett. **102**, 073007 (2009).
17. R. Velotta, N. Hay, M. B. Mason, M. Castillejo, and J. P. Marangos, Phys. Rev. Lett. **87**, 183901 (2001).
18. N. Hay, R. Velotta, M. Lein, R. de Nalda, E. Heesel, M. Castillejo, and J. P. Marangos, Phys. Rev. A **65**, 053805 (2002).
19. J. Itatani, D. Zeidler, J. Levesque, M. Spanner, D. M. Villeneuve, and P. B. Corkum, Phys. Rev. Lett. **94**, 123902 (2005).
20. T. Kanai, S. Minemoto, and H. Sakai, Phys. Rev. Lett. **98**, 053002 (2007).
21. S. Ramakrishna and T. Seideman, Phys. Rev. Lett. **99**, 113901 (2007).
22. Z. Yang, W. Cao, Y. Mo, H. Xu, K. Mi, P. Lan, Q. Zhang, and P. Lu, Natl. Sci. Rev. **8**, nwaa211 (2021).
23. A. Rupenyan, J. B. Bertrand, D. M. Villeneuve, and H. J. Wörner, Phys. Rev. Lett. **108**, 033903 (2012).
24. Y. He, L. He, P. Lan, B. Wang, L. Li, X. Zhu, W. Cao, and P. Lu, Phys. Rev. A **99**, 053419 (2019).
25. P. Huber-Wälchli, D. M. Guthals, and J. W. Nibler, Chem. Phys. Lett. **67**, 233 (1979).
26. M. D. Duncan, P. Österlin, and R. L. Byer, Opt. Lett. **6**, 90 (1981).
27. T. Lang, M. Motzkus, H. M. Frey, and P. Beaud, J. Chem. Phys. **115**, 5418 (2001).
28. T. Hornung, H. Skenderovic, K.-L. Kompa, and M. Motzkus, J. Raman Spectrosc. **35**, 934 (2004).
29. K. Yoshii, G. Miyaji, and K. Miyazaki, Opt. Lett. **34**, 1651 (2009).
30. Y. He, L. He, P. Wang, B. Wang, S. Sun, R. Liu, B. Wang, P. Lan, and P. Lu, Opt. Express **28**, 21182 (2020).
31. G. Karras, E. Hertz, F. Billard, B. Lavorel, J.-M. Hartmann, O. Faucher, E. Gershnabel, Y. Prior, and I. S. Averbukh, Phys. Rev. Lett. **114**, 153601 (2015).
32. H. Zhang, B. Lavorel, F. Billard, J.-M. Hartmann, E. Hertz, O. Faucher, J. Ma, J. Wu, E. Gershnabel, Y. Prior, and I. S. Averbukh, Phys. Rev. Lett. **122**, 193401 (2019).
33. G. Karras, E. Hertz, F. Billard, B. Lavorel, G. Siour, J.-M. Hartmann, O. Faucher, E. Gershnabel, Y. Prior, and I. S. Averbukh, Phys. Rev. A **94**, 033404 (2016).
34. K. Lin, P. Lu, J. Ma, X. Gong, Q. Song, Q. Ji, W. Zhang, H. Zeng, J. Wu, G. Karras, G. Siour, J.-M. Hartmann, O. Faucher, E. Gershnabel, Y. Prior, and I. S. Averbukh, Phys. Rev. X **6**, 041056 (2016).
35. K. Lin, J. Ma, X. Gong, Q. Song, Q. Ji, W. Zhang, H. Li, P. Lu, H. Li, H. Zeng, J. Wu, J.-M. Hartmann, O. Faucher, E. Gershnabel, Y. Prior, and I. S. Averbukh, Opt. Express **25**, 24917 (2017).
36. B. Wang, L. He, Y. He, Y. Zhang, R. Shao, P. Lan, and P. Lu, Opt. Express **27**, 30172 (2019).
37. D. Rosenberg, R. Damari, and S. Fleischer, Phys. Rev. Lett. **121**, 234101 (2018).
38. P. Wang, L. He, Y. He, S. Sun, R. Liu, B. Wang, P. Lan, and P. Lu, Opt. Express **29**, 663 (2021).
39. Z. Lian, Z. Hu, H. Qi, D. Fei, S. Luo, Z. Chen, and C.-C. Shu, Phys. Rev. A **104**, 053105 (2021).
40. D. Rosenberg, R. Damari, S. Kallush, and S. Fleischer, J. Phys. Chem. Lett. **8**, 5128 (2017).
41. J. Ma, H. Zhang, B. Lavorel, F. Billard, E. Hertz, J. Wu, C. Boulet, J.-M. Hartmann, and O. Faucher, Nat. Commun. **10**, 5780 (2019).
42. S. Fleischer, Y. Khodorkovsky, Y. Prior, and I. S. Averbukh, New J. Phys. **11**, 105039 (2009).
43. V. Renard, M. Renard, S. Guérin, Y. T. Pashayan, B. Lavorel, O. Faucher, and H. R. Jauslin, Phys. Rev. Lett. **90**, 153601 (2003).
44. V. Loriot, P. Tzallas, E. P. Benis, E. Hertz, B. Lavorel, D. Charalambidis, and O. Faucher, J. Phys. B: At., Mol. Opt. Phys. **40**, 2503 (2007).
45. K. Pandey and A. Singh, Int. J. Chem. Eng. Appl. **1**, 179 (2010).
46. J. Ma, L. H. Coudert, F. Billard, M. Bournazel, B. Lavorel, J. Wu, G. Maroulis, J.-M. Hartmann, and O. Faucher, Phys. Rev. Res. **3**, 023192 (2021).